HRI-RECAPP-2024-05

Explaining 95 GeV Anomalies in the 2-Higgs Doublet Model Type-I

Akshat Khanna,[1,*] Stefano Moretti,[2,3,†] and Agnivo Sarkar[4,‡]

[1] *Department of Physics, Indian Institute of Technology Gandhinagar, Gujarat 382055, India.*

[2] *School of Physics & Astronomy, University of Southampton, Highfield, Southampton SO17 1BJ, UK.*

[3] *Department of Physics & Astronomy, Uppsala University, Box 516, 75120 Uppsala, Sweden.*

[4] *Regional Centre for Accelerator-based Particle Physics, Harish-Chandra Research Institute, HBNI, Chhatnag Road, Jhunsi, Prayagraj (Allahabad) 211019, India*

arXiv:2409.02587v2 [hep-ph] 11 Dec 2025

We show how the 2-Higgs Doublet Model (2HDM) Type-I can explain some excesses recently seen at the Large Hadron Collider (LHC) in $\gamma\gamma$ and $\tau^+\tau^-$ final states in turn matching Large Electron Positron (LEP) data in $b\bar{b}$ signatures, all anomalies residing around 95 GeV. The explanation to such anomalous data is found in the aforementioned scenario when in inverted mass hierarchy, in two configurations: i) when the lightest CP-even Higgs state is alone capable of reproducing the excesses; ii) when a combination of such a state and the CP-odd Higgs boson is able to do so. To test further this scenario, we present some Benchmark Points (BPs) of it amenable to phenomenological investigation.

I. INTRODUCTION

A long-standing anomaly existing in LEP collider data [1] is the one hinting at the possibility of $e^+e^- \to Zh$ events being produced therein, with a Higgs boson state h with a mass of approximately 98 GeV decaying into $b\bar{b}$ pairs [2]. More recently, the CMS collaboration at the LHC has found an excess near 95 GeV in di-photon events in two separate analyses [3, 4]. In fact, they also reported an excess in $\tau^+\tau^-$ pairs, again, around a mass of about 98 GeV. Finally, ATLAS also observed an excess at around 95 GeV in di-photon events, thereby aligning with CMS, although, especially when including 'look elsewhere' effects, their findings are far less significant than the CMS ones. Altogether, in view of the limited mass resolution of the di-jet invariant mass at LEP, this older anomaly may well be consistent with the excesses seen by CMS (and, partially) ATLAS in the $\gamma\gamma$ and, even more so, $\tau^+\tau^-$ final states (as the mass resolution herein is also rather poor). As a consequence of this credible mass overlap, many studies [5–37] have tested the possibility of simultaneously fitting these excesses within Beyond the Standard Model (BSM) frameworks featuring a non-SM Higgs state lighter than 125 GeV, i.e., than the one observed at the LHC in 2012 [38, 39].

A possible route to follow in explaining such events through a companion Higgs state (to the 125 GeV one) is to resort to a 2HDM [40, 41], as done, e.g., in Refs. [42–45], wherein a Type-III (which allows direct couplings of both Higgs doublets to all SM fermions) with specific fermion textures was invoked successfully as a BSM explanation to the $b\bar{b}$, $\gamma\gamma$ and $\tau^+\tau^-$ excesses seen at LEP and the LHC. Herein, both a fully CP-even and a mixed CP-even/odd solution was found, upon refining the 2HDM Type-III Yukawa structure to comply with both theoretical consistency requirements and experimental measurements of the discovered Higgs mass and couplings (of the 125 GeV Higgs state).

In this study, we would like to analyse whether solutions of the same kind (i.e., both a fully CP-even and a mixed CP-even/odd one) can also be found in a 2HDM Type-I, wherein only one Higgs doublet gives mass to all SM fermions, again, satisfying the aforementioned theoretical requirements and experimental constraints.

The paper is organised as follows. In the next section, we briefly review the theoretical framework of the 2HDM Type-I. Then we discuss the theoretical and experimental constraints applied to such a BSM scenario in our study, which are described in section III. In section IV we show how the aforementioned configurations can naturally explain the discussed anomalous data. We then summarise our findings in section V.

* khanna_akshat@iitgn.ac.in
† s.moretti@soton.ac.uk; stefano.moretti@physics.uu.se
‡ agnivosarkar@hri.res.in

II. THE 2HDM TYPE-I

Among the various BSM scenarios, the 2HDM can be considered as a simple extension of the SM. In fact, the (pseudo)scalar sector of this model comprises two complex Higgs fields, ϕ_1 and ϕ_2, which transform as a doublet under the Electro-Weak (EW) gauge group $SU(2)_L \times U(1)_Y$ with hypercharge $Y = 1$. (For a detailed overview of this model interested reader can look into [46].) The most general gauge invariant CP-conserving scalar potential can be written as

$$\begin{aligned} V(\phi_1,\phi_2) = m_{11}^2\phi_1^\dagger\phi_1 + m_{22}^2\phi_2^\dagger\phi_2 - m_{12}^2\left[\phi_1^\dagger\phi_2 + \phi_2^\dagger\phi_1\right] + \frac{\lambda_1}{2}(\phi_1^\dagger\phi_1)^2 + \frac{\lambda_2}{2}(\phi_2^\dagger\phi_2)^2 \\ + \lambda_3(\phi_1^\dagger\phi_1)(\phi_2^\dagger\phi_2) + \lambda_4(\phi_1^\dagger\phi_2)(\phi_2^\dagger\phi_1) + \left[\frac{\lambda_5}{2}(\phi_1^\dagger\phi_2)^2 + h.c.\right] + \{\left[\lambda_6(\phi_1^\dagger\phi_1) + \lambda_7(\phi_2^\dagger\phi_2)\right](\phi_1^\dagger\phi_2) + h.c.\}. \end{aligned} \tag{1}$$

Given the hermiticity of the scalar potential, all the potential parameters of Eq. (1) must be real. In order to prevent tree level Flavour Changing Neutral Currents (FCNCs), one can postulate an additional discrete $\mathcal{Z}_2$ symmetry under which the scalar fields transform as $\phi_1 \to \phi_1$, $\phi_2 \to -\phi_2$. One then realises that the term proportional to m_{12}^2, λ_6 and λ_7 in Eq. (1) violates this $\mathcal{Z}_2$ symmetry explicitly. Therefore the potential can be expressed in the following form:

$$\begin{aligned} V(\phi_1,\phi_2) = m_{11}^2\phi_1^\dagger\phi_1 + m_{22}^2\phi_2^\dagger\phi_2 + \frac{\lambda_1}{2}(\phi_1^\dagger\phi_1)^2 + \frac{\lambda_2}{2}(\phi_2^\dagger\phi_2)^2 \\ + \lambda_3(\phi_1^\dagger\phi_1)(\phi_2^\dagger\phi_2) + \lambda_4(\phi_1^\dagger\phi_2)(\phi_2^\dagger\phi_1) + \{\frac{\lambda_5}{2}(\phi_1^\dagger\phi_2)^2 + h.c.\}. \end{aligned} \tag{2}$$

Both these Higgs fields, ϕ_1 and ϕ_2, acquire a non-zero Vacuum Expectation Value (VEV) (i.e., $\langle\phi_1\rangle = v_1$ and $\langle\phi_2\rangle = v_2$) and spontaneously break the EW gauge symmetry down to $U(1)_{\rm EM}$. After symmetry breaking, the $W^\pm$ and Z boson becomes massive and the (pseudo)scalar sector contains five physical Higgs bosons - two CP-even $\{H, h\}$, one CP-odd A and a pair of charged states $H^\pm$ with masses m_H, m_h, m_A and $m_{H^\pm}$, respectively. Both these VEVs v_1 and v_2 are related to the EW scale $v = \sqrt{v_1^2 + v_2^2} = 246$ GeV. The ratio between these two VEVs can be parameterised as $\tan\beta = \frac{v_2}{v_1}$. In addition, the mixing angle between the CP-even states $\{H, h\}$ can be parametrised as α. For the present study we consider the inverted hierarchy between the CP-even mass eigenstates. This particular choice alters the usual interpretation of the mass spectrum and the couplings[1]. Hereafter we align H as to be the SM like Higgs boson and h to be the lighter scalar state. In Eq. (3) we present the relations between the potential parameters λ_i's with the physical parameters of the model:

$$\begin{aligned} \lambda_1 &= \frac{c_\alpha^2 m_H^2 + s_\alpha^2 m_h^2}{v^2 c_\beta^2}, \\ \lambda_2 &= \frac{c_\alpha^2 m_h^2 + s_\alpha^2 m_H^2}{v^2 s_\beta^2}, \\ \lambda_3 &= \frac{(m_H^2 - m_h^2)s_\alpha c_\alpha - (\lambda_4+\lambda_5)v^2 c_\beta s_\beta}{v^2 c_\beta s_\beta}, \\ \lambda_4 &= \frac{m_A^2 - 2m_{H^\pm}^2}{v^2}, \\ \lambda_5 &= -\frac{m_A^2}{v^2}. \end{aligned} \tag{3}$$

The scalar potential given in Eq. (2) clearly has six independent parameters, so that the m_{ii}^2's can be traded off in terms of λ_i's using the extremisation conditions on the potential. We find relations of the parameters of the potentials given in Eq. (3) in terms of physical scalar masses and the angles $\{\beta, \alpha\}$, then use those as the input parameters for further analysis.

The right-handed up/down quarks and lepton fields are also charged under the aforementioned Z_2 symmetry and transform as $u_R^i \to -u_R^i$, $d_R^i \to -d_R^i$ and $\ell_R^i \to -\ell_R^i$, respectively. From these charge assignments one realises that all charged fermions exclusively couple to the Φ_2 field, leading to the traditional 2HDM Type-I scenario. In Eq. (4) we write down the Yukawa part of the Lagrangian in the mass eigenstate basis.

---

[1] For example, in the inverted mass hierarchy the alignment limit corresponds to $\cos(\beta-\alpha) \to 1$. However, we will not conform strictly to this limit in the present study.

$$-\mathcal{L}_{Yukawa} = + \sum_{f=u,d,\ell} \left[m_f f \bar{f} + \left(\frac{m_f}{v} \kappa_h^f \bar{f} f h + \frac{m_f}{v} \kappa_H^f \bar{f} f H - i \frac{m_f}{v} \kappa_A^f \bar{f} \gamma_5 f A \right) \right] + \frac{\sqrt{2}}{v} \bar{u} \left(m_u V \kappa_{H^+}^u P_L + V m_d \kappa_{H^+ P_R}^d \right) d H^+ + \frac{\sqrt{2} m_\ell \kappa_{H^+}^\ell}{v} \bar{\nu}_L \ell_R H^+ + h.c. \tag{4}$$

Here m_f is the fermion mass, V is the Cabibbo-Kobayashi-Maskawa (CKM) matrix and $P_{L/R} = \frac{1 \pm \gamma_5}{2}$ are the projection operators. The explicit form of the scaling functions κ_i's (also called coupling modifiers) are detailed in Table.I.

κ_S^i	Coefficient
κ_H^V	$\cos(\beta - \alpha)$
κ_h^V	$\sin(\beta - \alpha)$
κ_H^f	$\frac{\sin\alpha}{\sin\beta}$
κ_h^f	$\frac{\cos\alpha}{\sin\beta}$
κ_A^f	$\cot\beta$
$\kappa_{H^+}^u$	$\cot\beta$
$\kappa_{H^+}^{d/\ell}$	$-\cot\beta$

TABLE I: Explicit form of different coupling modifiers κ_S^i. Here S denotes different scalars in the 2HDM and i can be SM gauge bosons and fermions.

III. CONSTRAINTS

In this section, we describe different theoretical and experimental constraints which are required to restrict the parameter space of the 2HDM Type-I.

A. Theoretical Constraints

- **Vacuum Stability:** The vacuum stability conditions ensure that the potential must be bounded from below in all possible field direction. To achieve this, the λ_i parameters must follow certain relationships such that the quartic terms in the potential must dominate for large field values. Here we list down the conditions on the λ_i's which are needed to meet the stability criteria, which prevents the potential from becoming infinitely negative, [47]

$$\lambda_1 > 0, \quad \lambda_2 > 0, \quad \lambda_3 + \sqrt{\lambda_1 \lambda_2} > 0, \quad \lambda_3 + \lambda_4 - |\lambda_5| + \sqrt{\lambda_1 \lambda_2} > 0.$$

- **Unitarity:** The unitarity constraints are necessary to ensure that the theory remains predictive at high energies. At tree level, unitarity imposes specific conditions on the energy growth of all possible $2 \to 2$ scattering processes. Ref. [48, 49] derives the unitarity conditions for the 2HDM model explicitly. According to the unitarity constraint, the following relations should be obeyed:

$$|u_i| \leq 8\pi,$$

where

$$\begin{aligned}
u_1 &= \frac{1}{2}(\lambda_1 + \lambda_2 \pm \sqrt{(\lambda_1 - \lambda_2)^2 + 4|\lambda_5|^2}), \\
u_2 &= \frac{1}{2}(\lambda_1 + \lambda_2 \pm \sqrt{(\lambda_1 - \lambda_2)^2 + 4\lambda_4^2}), \\
u_3 &= \frac{1}{2}(3(\lambda_1 + \lambda_2) \pm \sqrt{9(\lambda_1 - \lambda_2)^2 + 4(2\lambda_3 + \lambda_4)^2}), \\
u_4 &= \lambda_3 + 2\lambda_4 \pm 3|\lambda_5|, \\
u_5 &= \lambda_3 \pm |\lambda_5|, \\
u_6 &= \lambda_3 \pm \lambda_4.
\end{aligned}$$

- **Perturbativity:** The perturbativity condition on the parameters of the Higgs potential, which imposes an upper limit on all the quartic couplings, demands that, for all i values, one has $\lambda_i \leq |4\pi|$.

B. Experimental Constraints

- **EW Precision Tests** We evaluated the EW precision constraints by computing the S, T and U parameters using the SPheno package [50], with the model files written in SARAH [51]. These so-called 'oblique parameters' provide stringent constraints on new physics masses and relevant couplings. Therefore any BSM theory should conform to these precision data which are primarily collected by LEP, SLC and Tevatron. The numerical values, with correlation coefficients of +0.92 between S and T plus −0.68 (−0.87) between S and U (T and U) are [52]

$$S = 0.04 \pm 0.11, \quad T = 0.09 \pm 0.14, \quad U = -0.02 \pm 0.11.$$

- **BSM Higgs Boson Exclusions** We assessed the exclusion limits from direct searches for BSM (pseudo)scalars states at the LEP, Tevatron and the LHC. These exclusion limits were evaluated at the 95% Confidence Level (C.L.) using the HiggsBounds-6 [53] module via the HiggsTools [54] package. In our analysis we have also demanded that our lighter Higgs must comply with the results of [55], where the Higgs particles are produced in association with a massive vector boson or a top anti-quark pair and further decays via leptonic modes.

- **SM-Like Higgs Boson Discovery** We examined the compatibility of our 125 GeV Higgs boson with the discovered SM-like Higgs boson using a goodness-of-fit test. Specifically, we calculated the χ-square value with HiggsSignals-3 [56] via HiggsTools, comparing the predicted signal strengths of our Higgs boson to those observed experimentally. We retained the parameter spaces that satisfies the condition $\chi^2_{125} < 189.42$ [44, 45], corresponding to a 95% C.L. with 159 degrees of freedom. The choice of the upper bound on $\chi^2 < 189.42$, corresponds to a global χ^2 goodness of fit test at 95% C.L. ensuring that the predicted properties of the heavier CP even Higgs state (with the mass $m_H = 125$ GeV) of the underlying 2HDM Type-I closely match those of the Higgs boson observed at the LHC, thereby keeping the model compatible under current experimental constraints.

- **Flavour Physics** We incorporated constraints from B-physics observables, which are sensitive to potential new physics contributions in loop mediated FCNC processes. Specifically, we tested the most stringent bound on the Branching Ratio ($\mathcal{BR}$) of the $B \to X_s\gamma$ decay using Next-to-Leading Order (NLO) calculations in QCD as discussed in [57]:

$$\mathcal{BR}(B \to X_s\gamma) = \frac{\Gamma(B \to X_s\gamma)}{\Gamma_{SL}} \mathcal{BR}_{SL} \tag{5}$$

where $\mathcal{BR}_{\rm SL}$ is the semi-leptonic $\mathcal{BR}$ and Γ_{SL} is the semi-leptonic decay width.

We took our input parameters from the most recent Particle Data Group (PDG) compilation [58], as follows:

$$\begin{aligned}
\alpha_s(M_Z) &= 0.1179 \pm 0.0010, & m_t &= 172.76 \pm 0.3, \\
\frac{m_b}{m_c} &= 4.58 \pm 0.01, & \alpha &= \frac{1}{137.036}, \\
\mathcal{BR}_{\rm SL} &= 0.1049 \pm 0.0046, & |\frac{V_{ts}^* V_{tb}}{V_{cb}}|^2 &= 0.95 \pm 0.02, \\
m_b(\overline{\rm MS}) &= 4.18 \pm 0.03, & m_c &= 1.27 \pm 0.02, \\
m_Z &= 91.1876 \pm 0.0021, & m_W &= 86.377 \pm 0.012.
\end{aligned}$$

The following restriction has been imposed, which represents the 3σ experimental limit:

$$2.87 \times 10^{-4} < \mathcal{BR}(B \to X_s\gamma) < 3.77 \times 10^{-4}.$$

Other B-physics observables, like $\mathcal{BR}(B^+ \to \tau^+\nu_\tau)$, $\mathcal{BR}(D_s \to \tau\nu_\tau)$, $\mathcal{BR}(B_s \to \mu^+\mu^-)$ and $\mathcal{BR}(B^0 \to \mu^+\mu^-)$ have been taken care of by using the FlavorKit tool [59] provided by the SPheno package [50]. Our calculated $b \to s\gamma$ results were also found to be consistent with the FlavorKit tool.

IV. EXPLAINING THE ANOMALIES

The primary objective of this paper is to investigate whether the 2HDM Type-I can explain the excesses observed at the LHC and in LEP data over the $94-96$ GeV mass range. To do so, we need to define the signal strength corresponding to these three excesses. The signal strength is formulated as a ratio between the observed number of events to the expected number of events for a hypothetical SM Higgs state of mass 95 GeV. Assuming the Narrow Width Approximation (NWA), the signal strength for the $\tau^+\tau^-, \gamma\gamma$ and $b\bar{b}$ channels can be parameterised as cross section (σ) times $\mathcal{BR}$, as follows:

$$\begin{aligned}
\mu_{\tau^+\tau^-}(\phi) &= \frac{\sigma_{\rm 2HDM}(gg\to\phi)}{\sigma_{\rm SM}(gg\to h_{\rm SM})} \times \frac{\mathcal{BR}_{\rm 2HDM}(\phi\to\tau^+\tau^-)}{\mathcal{BR}_{\rm SM}(h_{\rm SM}\to\tau^+\tau^-)},\\
\mu_{\gamma\gamma}(\phi) &= \frac{\sigma_{\rm 2HDM}(gg\to\phi)}{\sigma_{\rm SM}(gg\to h_{\rm SM})} \times \frac{\mathcal{BR}_{\rm 2HDM}(\phi\to\gamma\gamma)}{\mathcal{BR}_{\rm SM}(h_{\rm SM}\to\gamma\gamma)},\\
\mu_{b\bar{b}}(\phi) &= \frac{\sigma_{\rm 2HDM}(e^+e^-\to Z\phi)}{\sigma_{\rm SM}(e^+e^-\to Zh_{\rm SM})} \times \frac{\mathcal{BR}_{\rm 2HDM}(\phi\to b\bar{b})}{\mathcal{BR}_{\rm SM}(h_{\rm SM}\to b\bar{b})}.
\end{aligned} \tag{6}$$

Here, $h_{\rm SM}$ corresponds to a SM like Higgs Boson with a mass of 95 GeV while ϕ is a 2HDM Type-I Higgs state with the same mass. The experimental measurements for these three signal strengths around 95 GeV are expressed as

$$\begin{aligned}
\mu^{\rm exp}_{\gamma\gamma} &= \mu^{\rm ATLAS+CMS}_{\gamma\gamma} = 0.24^{+0.09}_{-0.08},\ [3, 60, 61]\\
\mu^{\rm exp}_{\tau^+\tau^-} &= 1.2\pm0.5,\ [62]\\
\mu^{\rm exp}_{b\bar{b}} &= 0.117\pm0.057.\ [1, 63]
\end{aligned} \tag{7}$$

Although the ditau excess is most prominent around 100 GeV and the $b\bar{b}$ excess near 98 GeV, a search around 95 GeV could provide a unified explanation for all these three anomalies. This is because the mass resolution in the ditau final states is substantially large and the LEP excess, associated with the $b\bar{b}$ final states, is also rather broad: therefore, a common origin for these excesses may plausibly reside around 95 GeV [20].

In our analysis, we have combined the di-photon measurements from the ATLAS and CMS experiments, denoted as $\mu^{\rm ATLAS}_{\gamma\gamma}$ and $\mu^{\rm CMS}_{\gamma\gamma}$, respectively. The ATLAS measurement yields a central value of 0.18 ± 0.1 [64] while the CMS measurement yields a central value of $0.33^{+0.19}_{-0.12}$ [65]. The combined measurement, denoted by $\mu^{\rm ATLAS+CMS}_{\gamma\gamma}$ is determined by taking the average of these two central values, assuming these measurements are uncorrelated. The corresponding combined uncertainty is calculated by adding the individual uncertainties in quadrature. To determine whether the observed excess can be explained through our model or otherwise, we perform a χ^2 analysis using the central values $\mu^{\rm exp}$ and the 1σ uncertainties $\Delta\mu^{\rm exp}$ associated with the signal related to the excesses as defined in Eq. (7). The contribution to the χ^2 for each of the channel is calculated using the equation

$$\chi^2_{\gamma\gamma,\tau^+\tau^-,b\bar{b}} = \frac{(\mu_{\gamma\gamma,\tau^+\tau^-,b\bar{b}}(\phi) - \mu^{\rm exp}_{\gamma\gamma,\tau^+\tau^-,b\bar{b}})^2}{(\Delta\mu^{\rm exp}_{\gamma\gamma,\tau^+\tau^-,b\bar{b}})^2}. \tag{8}$$

Hence, the resulting χ^2, which we will use to determine if the excesses can be achieved by the allowed region of the parameter space of 2HDM Type-I, or otherwise, is the following:

$$\chi^2_{\gamma\gamma,\tau^+\tau^-,b\bar{b}} = \chi^2_{\gamma\gamma} + \chi^2_{\tau^+\tau^-} + \chi^2_{b\bar{b}}. \tag{9}$$

We test this BSM scenario for two cases: firstly, we consider both the CP-even and CP-odd Higgs states simultaneously (i.e., $\phi = h + A$, except for $b\bar{b}$ where $\phi = h$ as the CP-odd scalar A does not couple to ZZ mode) in explaining the anomaly and, secondly, we only exploit the CP-even Higgs state (i.e., $\phi = h$) in order to explain it. Hence, we align our H state (recall that we have $m_h < m_H$) with the SM Higgs boson, so that $m_H = 125$ GeV, and start a Monte Carlo (MC) sampling of the various input parameters.

A. The Overlapping Solution

In the case of the overlapping solution, the signal strengths corresponding to the $\tau^+\tau^-$ and $\gamma\gamma$ channels receive substantial contribution from both the CP-even and CP-odd states simultaneously[2]. In contrast, for the $b\bar{b}$ mode only

[2] Here we have considered a CP-conserving potential. As a result, the h and A states would not interfere with each other.

Parameter	Scan Range
m_H	125 GeV
m_h	94 GeV – 96 GeV
m_A	94 GeV – 96 GeV
$m_{H^\pm}$	140 GeV – 250 GeV
$\tan\beta$	0.5 – 100
$\sin(\beta-\alpha)$	−0.60 – 0.60

TABLE II: The scan range which is used for the MC sampling for the overlapping solution.

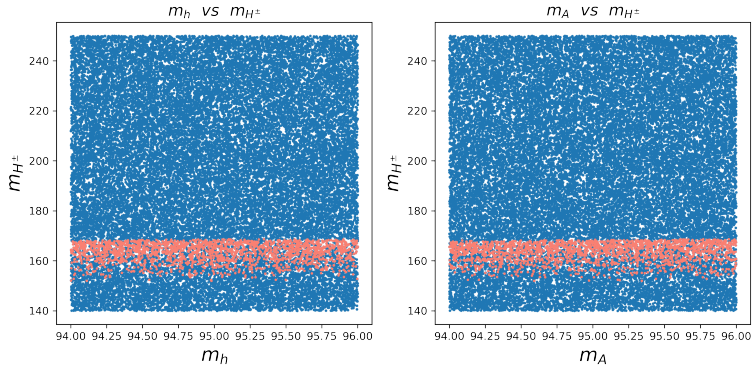


FIG. 1: Results of the scan in Table II mapped against the Higgs boson masses. The blue regions are allowed by stability, unitarity and perturbativity constraints while the red regions are allowed by Higgs data, $b \to s\gamma$ and EW precision constraints.

the CP-even state contribute as the trilinear coupling AZZ is zero at tree level. As a result, the signal strengths can be expressed in the following manner:

$$\mu_{\tau^+\tau^-}(h+A) = \mu_{\tau^+\tau^-}(h) + \mu_{\tau^+\tau^-}(A), \quad \mu_{\gamma\gamma}(h+A) = \mu_{\gamma\gamma}(h) + \mu_{\gamma\gamma}(A), \quad \mu_{b\bar{b}}(h).$$

We generated MC samples in the scan range as described in Table II. After testing them against various theoretical and experimental constraints, the allowed parameter space is illustrated in Figure 1. The region of the parameter space that pass the theoretical constraints are depicted by the blue points while the region that pass the experimental constraints are depicted by red points. The plot illustrates that a nearly degenerate solution with both the CP-even and CP-odd Higgs in the $94-96$ GeV mass range is viable for the charged Higgs mass ranging over the interval $152\ \text{GeV} < m_H^\pm < 168\ \text{GeV}$. We will use the overlapping region of the two coloured point distributions to test the aforementioned anomalies.

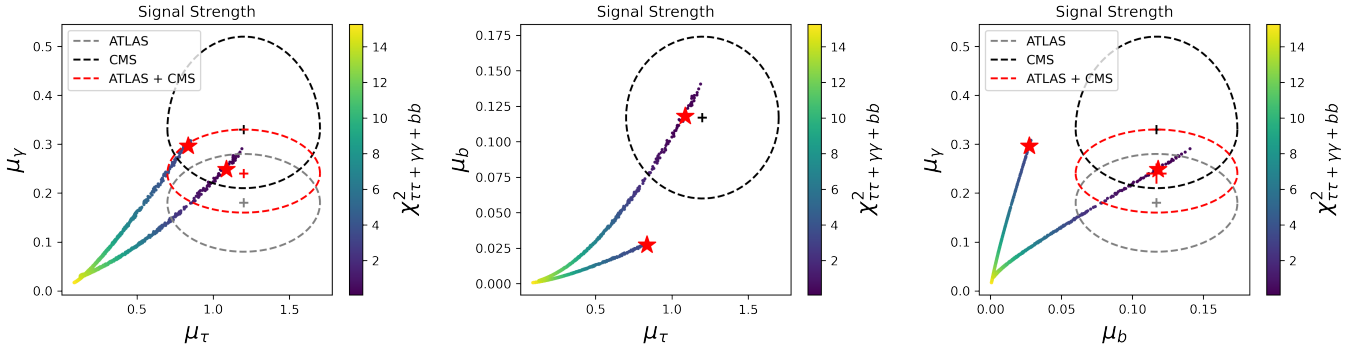


FIG. 2: Correlations amongst the signal strengths in Eq. (6). Here, the total χ^2 is displayed using the colour bar and the best fit point is given by the star marker. The ATLAS and CMS results with their corresponding 1σ band are also represented.

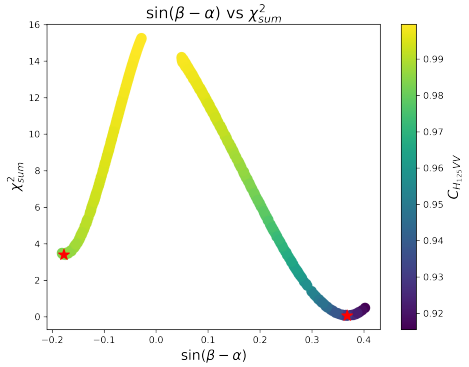


FIG. 3: The value of $\sin(\beta-\alpha)$ plotted against $\chi^2_{\rm sum}$. The $\chi^2_{\rm min}$ is indicated by a star. The color gradient represents the strength of the coupling between the SM like Higgs boson and the pair of vector bosons.

Figure 2 illustrates the total χ^2 distribution for points that are compatible with all three anomalies and the best fit point is marked by a star, corresponding to $\chi^2_{\rm min}$. The experimentally observed signal strength with their 1σ band is also superimposed in the plot to test them against this model's best fit point. The chi-square fit reveals two distinct branches, differentiated by the sign of $\sin(\beta-\alpha)$. The longer branch is characterised by the positive values, while the smaller one by the negative values. Figure 3 further highlights the sign of the EW coupling parameter, with the best-fit point in both branches again marked by a red star. Notably, the positive branch contains a best fit point that simultaneously explains all the three anomalies within the 1σ region. However, an analysis by the ATLAS collaboration on the 2HDM Type-I [66] imposes significant restrictions on the positive region of the value $\sin(\beta-\alpha)$, limiting its viability. The negative branch also allows for a simultaneous explanation of all the three anomalies within the 1σ region. However, when the $b\bar{b}$ channel anomaly is examined in isolation, it cannot be explained at the 1σ level. While the vector boson coupling with the SM Higgs boson, indicated by the colour bar, is weakened as in this case, it remains within the allowed range.

Given that the di-photon excess is most pronounced around 95 GeV, we also plot the allowed points within the $94-96$ GeV range over the CMS and ATLAS results for the signal strength in the $\gamma\gamma$ channel, for the negative branch, as shown in Figure 4. The expected and observed CMS limits are shown by the black dashed and solid lines. The green and yellow bands indicate the 1σ and 2σ uncertainties and the plot is overlaid by the ATLAS observed 95% C.L. limits on the signal strength with the red dashed and solid lines. The combined signal strength (CMS+ATLAS) at 95.4 GeV with its error bar is also shown using a red dot. The points explaining the anomaly at the 1σ level, for 3 degrees of freedom, corresponding to the $\gamma\gamma$, $\tau\tau$ and $b\bar{b}$ channels as shown in Eq. (9), which requires $\chi^2 < 3.53$, are plotted in dark red while the points explaining it at the 2σ level, demanding $\chi^2 < 7.8147$, are shown in peru colour. (Less likely points are given in sky blue.) The best fit point in the $94-96$ range is also indicated using midnight blue color. It can be clearly seen that many parameter points are suited to explain the excesses observed. The details of the best fit point as marked in the figure is shown in Table III. Although we have imposed a global χ^2 goodness of test at 95% C.L., the best-fit BP listed in Table III yields a χ^2 value of 171.14, , which also falls within the 3σ region corresponding to the more stringent HiggsSignals constraint, $\chi^2 \leq \chi^2_{\rm SM} + 11.83$.

B. The Single Solution

In this case, only the h state is responsible for explaining all the three anomalies. We sampled points for the scan ranges described in Table IV and the points that pass the various constraints are depicted in Figure 5, wherein

Parameter	m_H	m_h	m_A	$m_{H^\pm}$	$\tan\beta$	$\sin(\beta-\alpha)$	$\mu_{\tau^+\tau^-}(h+A)$	$\mu_{\gamma\gamma}(h+A)$	$\mu_{b\bar{b}}(h)$	$\chi^2_{\tau^+\tau^-+\gamma\gamma+b\bar{b}}$
Figure 2	125.0	94.36	94.44	166.63	2.33	−0.17	0.836	0.296	0.027	3.402

TABLE III: BP extracted from Figure 2 corresponding to the negative region of $\sin(\beta-\alpha)$. The masses of the Higgs states are given in units of GeV. The positive region of $\sin(\beta-\alpha)$ is strongly constrained by the ATLAS analysis of the 2HDM Type-I [66], rendering it less viable.

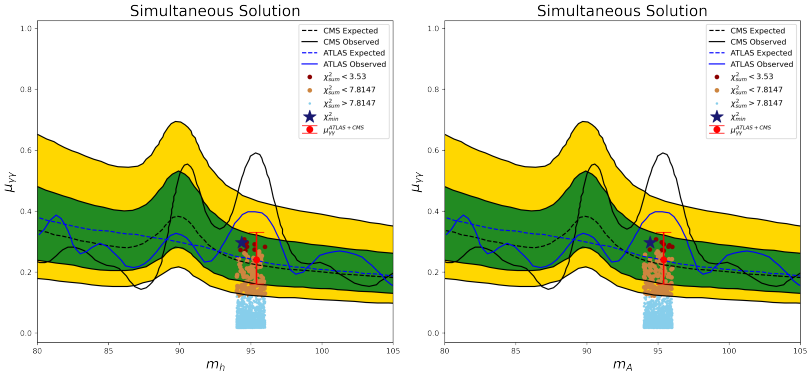


FIG. 4: The di-photon signal strength results from experiment tensioned against the 2HDM Type-I predictions satisfying the three anomalies simultaneously.

Parameter	Scan Range
m_H	125 GeV
m_h	94 GeV – 96 GeV
m_A	90 GeV – 250 GeV
$m_{H^\pm}$	140 GeV – 250 GeV
$\tan\beta$	0.5 – 100
$\sin(\beta-\alpha)$	−0.60 – 0.60

TABLE IV: The scan range which is used for the MC sampling for the single solution.

the blue shaded region indicates the points that pass the various theoretical constraints while the red shaded region indicates the part of parameter space that survives after imposing different experimental bounds. The plots clearly represent the allowed parameter space for the CP-odd and charged Higgs masses, given that we fix our CP-even mass to lie in the range 94 – 96 GeV. Although the charged Higgs mass is bounded at around 155 GeV, the CP-odd one covers almost the entire scan range. The plots also clearly illustrate the degeneracy between the CP-odd and the charged Higgs states, which is required to satisfy the EW precision constraints. Note that the allowed CP-odd scalar mass also lies within the 94 GeV to 96 GeV mass window, hinting to the overlapping solution that we discussed in the previous section. We move ahead with testing the allowed points with the observed anomalies.

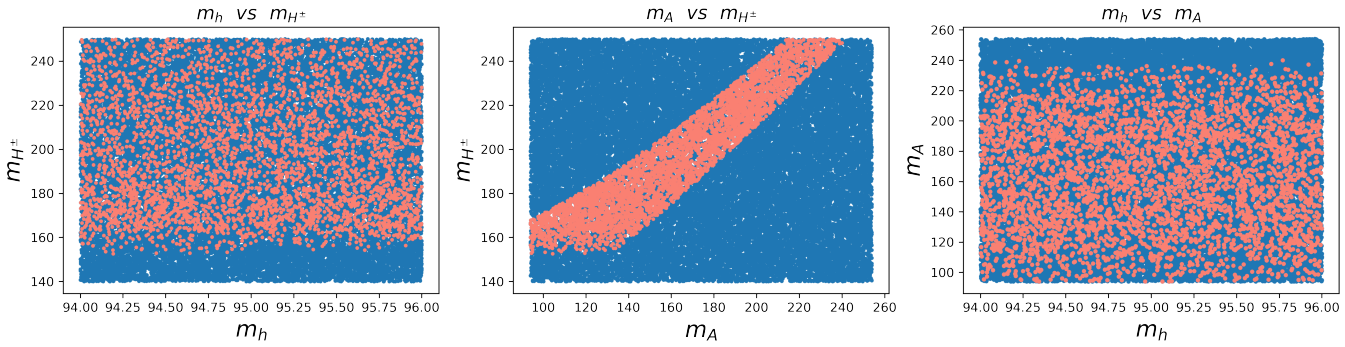


FIG. 5: Results of the scan in Table IV mapped against the Higgs masses. The blue regions are allowed by stability, unitarity and perturbativity constraints while the red regions are allowed by Higgs data, $b \to s\gamma$ and EW precision constraints.

The total χ^2 fit for the points passing all the constraints is displayed in Figure 6, wherein the best fit point (i.e., again, the $\chi^2_{\rm min}$ one) is indicated with a star. We have again overlaid the plot with the experimentally observed data within the 1σ band. Here again the branches are differentiated by the sign of $\sin(\beta-\alpha)$, with the larger branch depicting the positive while the smaller one depicting the negative values. The plot demonstrates that, while a simultaneous solution exists for all three cases in the positive branch, no point in the negative branch satisfies all three

anomalies simultaneously within the 2σ level ($\chi^2 < 7.8147$), once the ATLAS constraint is imposed. Nevertheless, viable points do appear in the negative branch when the requirement is relaxed to the 3σ level ($\chi^2 < 14.156$). Figure 7 provides additional insight into the sign of the electroweak coupling parameter, with red stars denoting the best-fit points in each of the two branches.

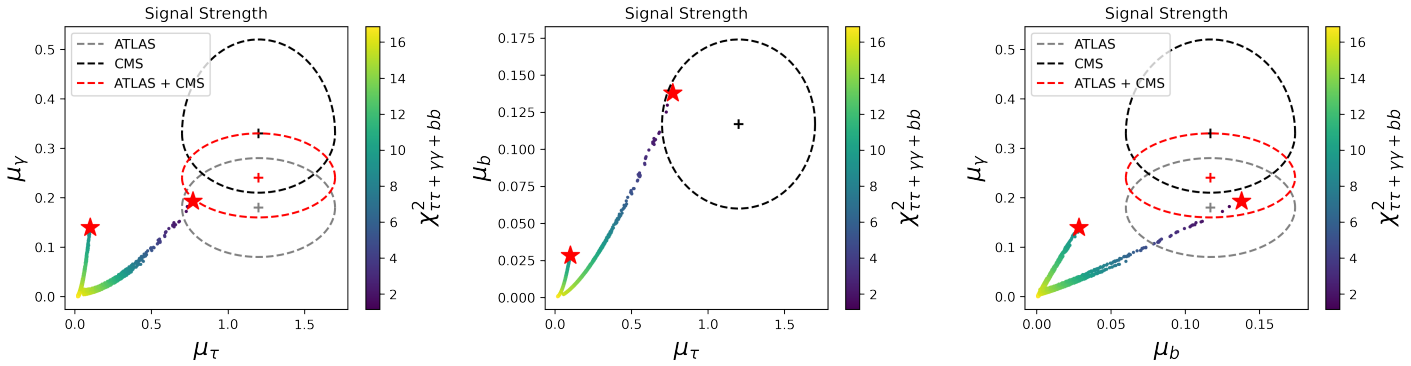


FIG. 6: Correlations amongst the signal strengths in Eq. (6). Here, the total χ^2 is displayed using the colour bar and the best fit point is given by star marker. ATLAS and CMS results with their corresponding 1σ bands are also added.

V. CONCLUSIONS

In summary, we have proven that somewhat anomalous data produced at LEP and the LHC in $b\bar{b}$ as well as $\tau^+\tau^-$ and $\gamma\gamma$ final states, respectively, all clustering in a mass window around 95 GeV, are consistent with the possibility of the 2HDM Type-I in inverted mass hierarchy (i.e., $m_H = 125$ GeV) explaining these through one of its neutral Higgs states. Specifically, only one configuration is possible: the one where both the (degenerate) h and A states cooperate to explain the aforementioned anomalies, if we take the ATLAS result into account. This is an intriguing finding, as such a Higgs state can also be probed in collateral signatures specific to the 2HDM Type-I in inverted mass hierarchy, as emphasised in various previous literature [67–74]. To aid testing this theoretical hypothesis, we have produced a BP amenable to further phenomenological analysis, wherein the parameter space point is giving the best fit to all anomalies. We also found that there does not exist a solution for only the CP-even case, that could explain the three anomalies simultaneously in the 2HDM Type-I even within 2σ.

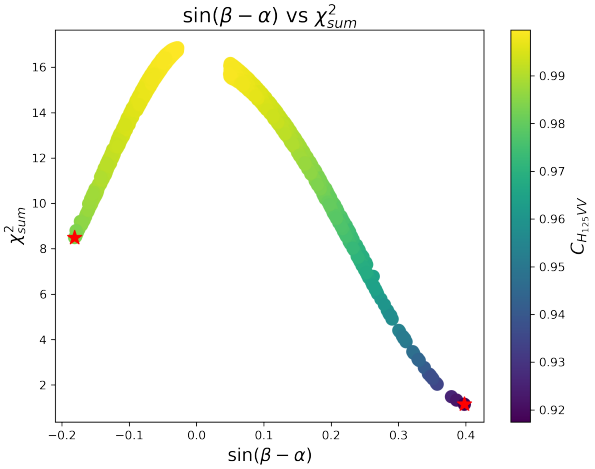


FIG. 7: The value of $\sin(\beta-\alpha)$ plotted against $\chi^2_{\rm sum}$. The best fit point is indicated by a star. The color gradient represents the strength of the coupling between the SM like 125 GeV Higgs boson and the pair of vector bosons.

ACKNOWLEDGMENTS

The work of S.M. is supported in part through the NExT Institute and the STFC Consolidated Grant ST/X000583/1. A.S. acknowledges the support from SERB-National Postdoctoral fellowship (Ref No: PDF/2023/002572). A.K. acknowledges the support from Director's Fellowship at IIT Gandhinagar. All authors thank Tanmoy Mondal and Prasenjit Sanyal for their help in discovering a mistake in their calculations.

[1] R. Barate *et al.* (LEP Working Group for Higgs boson searches, ALEPH, DELPHI, L3, OPAL), Search for the standard model Higgs boson at LEP, Phys. Lett. B **565**, 61 (2003), arXiv:hep-ex/0306033.
[2] S. Schael *et al.* (ALEPH, DELPHI, L3, OPAL, LEP Working Group for Higgs Boson Searches), Search for neutral MSSM Higgs bosons at LEP, Eur. Phys. J. C **47**, 547 (2006), arXiv:hep-ex/0602042.
[3] A. M. Sirunyan *et al.* (CMS), Search for a standard model-like Higgs boson in the mass range between 70 and 110 GeV in the diphoton final state in proton-proton collisions at $\sqrt{s} = 8$ and 13 TeV, Phys. Lett. B **793**, 320 (2019), arXiv:1811.08459 [hep-ex].
[4] CMS Collaboration (CMS), Search for a standard model-like Higgs boson in the mass range between 70 and 110 GeV in the diphoton final state in proton-proton collisions at $\sqrt{s} = 13$ TeV, https://cds.cern.ch/record/2852907/, CERN, Geneva (2023).
[5] J. Cao, X. Guo, Y. He, P. Wu, and Y. Zhang, Diphoton signal of the light Higgs boson in natural NMSSM, Phys. Rev. D **95**, 116001 (2017), arXiv:1612.08522 [hep-ph].
[6] S. Heinemeyer, C. Li, F. Lika, G. Moortgat-Pick, and S. Paasch, Phenomenology of a 96 GeV Higgs boson in the 2HDM with an additional singlet, Phys. Rev. D **106**, 075003 (2022), arXiv:2112.11958 [hep-ph].
[7] T. Biekötter, A. Grohsjean, S. Heinemeyer, C. Schwanenberger, and G. Weiglein, Possible indications for new Higgs bosons in the reach of the LHC: N2HDM and NMSSM interpretations, Eur. Phys. J. C **82**, 178 (2022), arXiv:2109.01128 [hep-ph].
[8] T. Biekötter, M. Chakraborti, and S. Heinemeyer, A 96 GeV Higgs boson in the N2HDM, Eur. Phys. J. C **80**, 2 (2020), arXiv:1903.11661 [hep-ph].
[9] J. Cao, X. Jia, Y. Yue, H. Zhou, and P. Zhu, 96 GeV diphoton excess in seesaw extensions of the natural NMSSM, Phys. Rev. D **101**, 055008 (2020), arXiv:1908.07206 [hep-ph].
[10] T. Biekötter, S. Heinemeyer, and G. Weiglein, Excesses in the low-mass Higgs-boson search and the W-boson mass measurement, Eur. Phys. J. C **83**, 450 (2023), arXiv:2204.05975 [hep-ph].
[11] S. Iguro, T. Kitahara, and Y. Omura, Scrutinizing the $95-100$ GeV di-tau excess in the top associated process, Eur. Phys. J. C **82**, 1053 (2022), arXiv:2205.03187 [hep-ph].
[12] W. Li, H. Qiao, and J. Zhu, Light Higgs boson in the NMSSM confronted with the CMS di-photon and di-tau excesses*, Chin. Phys. C **47**, 123102 (2023), arXiv:2212.11739 [hep-ph].
[13] J. M. Cline and T. Toma, Pseudo-Goldstone dark matter confronts cosmic ray and collider anomalies, Phys. Rev. D **100**, 035023 (2019), arXiv:1906.02175 [hep-ph].
[14] T. Biekötter and M. O. Olea-Romacho, Reconciling Higgs physics and pseudo-Nambu-Goldstone dark matter in the S2HDM using a genetic algorithm, JHEP **10**, 215, arXiv:2108.10864 [hep-ph].
[15] A. Crivellin, J. Heeck, and D. Müller, Large $h \to bs$ in generic two-Higgs-doublet models, Phys. Rev. D **97**, 035008 (2018), arXiv:1710.04663 [hep-ph].
[16] G. Cacciapaglia, A. Deandrea, S. Gascon-Shotkin, S. Le Corre, M. Lethuillier, and J. Tao, Search for a lighter Higgs boson in Two Higgs Doublet Models, JHEP **12**, 068, arXiv:1607.08653 [hep-ph].
[17] A. A. Abdelalim, B. Das, S. Khalil, and S. Moretti, Di-photon decay of a light Higgs state in the BLSSM, Nucl. Phys. B **985**, 116013 (2022), arXiv:2012.04952 [hep-ph].
[18] T. Biekötter, S. Heinemeyer, and G. Weiglein, Mounting evidence for a 95 GeV Higgs boson, JHEP **08**, 201, arXiv:2203.13180 [hep-ph].
[19] T. Biekötter, S. Heinemeyer, and G. Weiglein, The CMS di-photon excess at 95 GeV in view of the LHC Run 2 results, Phys. Lett. B **846**, 138217 (2023), arXiv:2303.12018 [hep-ph].
[20] D. Azevedo, T. Biekötter, and P. M. Ferreira, 2HDM interpretations of the CMS diphoton excess at 95 GeV, JHEP **11**, 017, arXiv:2305.19716 [hep-ph].
[21] T. Biekötter, S. Heinemeyer, and G. Weiglein, 95.4 GeV diphoton excess at ATLAS and CMS, Phys. Rev. D **109**, 035005 (2024), arXiv:2306.03889 [hep-ph].
[22] J. Cao, X. Jia, and J. Lian, Unified interpretation of the muon g-2 anomaly, the 95 GeV diphoton, and $b\bar{b}$ excesses in the general next-to-minimal supersymmetric standard model, Phys. Rev. D **110**, 115039 (2024), arXiv:2402.15847 [hep-ph].
[23] K. Wang and J. Zhu, 95 GeV light Higgs in the top-pair-associated diphoton channel at the LHC in the minimal dilaton model*, Chin. Phys. C **48**, 073105 (2024), arXiv:2402.11232 [hep-ph].
[24] W. Li, H. Qiao, K. Wang, and J. Zhu, Light dark matter confronted with the 95 gev diphoton excess (2023), arXiv:2312.17599 [hep-ph].
[25] P. S. B. Dev, R. N. Mohapatra, and Y. Zhang, Explanation of the 95 GeV $\gamma\gamma$ and $b\bar{b}$ excesses in the minimal left-right symmetric model, Phys. Lett. B **849**, 138481 (2024), arXiv:2312.17733 [hep-ph].

[26] D. Borah, S. Mahapatra, P. K. Paul, and N. Sahu, Scotogenic $U(1)_{L_\mu - L_\tau}$ origin of $(g-2)_\mu$, W-mass anomaly and 95 GeV excess, Phys. Rev. D **109**, 055021 (2024), arXiv:2310.11953 [hep-ph].

[27] J. Cao, X. Jia, J. Lian, and L. Meng, 95 GeV diphoton and $b\bar{b}$ excesses in the general next-to-minimal supersymmetric standard model, Phys. Rev. D **109**, 075001 (2024), arXiv:2310.08436 [hep-ph].

[28] U. Ellwanger and C. Hugonie, Additional Higgs Bosons near 95 and 650 GeV in the NMSSM, Eur. Phys. J. C **83**, 1138 (2023), arXiv:2309.07838 [hep-ph].

[29] J. A. Aguilar-Saavedra, H. B. Câmara, F. R. Joaquim, and J. F. Seabra, Confronting the 95 GeV excesses within the U(1)'-extended next-to-minimal 2HDM, Phys. Rev. D **108**, 075020 (2023), arXiv:2307.03768 [hep-ph].

[30] S. Ashanujjaman, S. Banik, G. Coloretti, A. Crivellin, B. Mellado, and A.-T. Mulaudzi, $SU(2)_L$ triplet scalar as the origin of the 95 GeV excess?, Phys. Rev. D **108**, L091704 (2023), arXiv:2306.15722 [hep-ph].

[31] J. Dutta, J. Lahiri, C. Li, G. Moortgat-Pick, S. F. Tabira, and J. A. Ziegler, Dark matter phenomenology in 2HDMS in light of the 95 GeV excess, Eur. Phys. J. C **84**, 926 (2024), arXiv:2308.05653 [hep-ph].

[32] U. Ellwanger and C. Hugonie, Nmssm with correct relic density and an additional 95 GeV Higgs boson, Eur. Phys. J. C **84**, 526 (2024), arXiv:2403.16884 [hep-ph].

[33] M. A. Diaz, G. Cerro, S. Dasmahapatra, and S. Moretti, Bayesian active search on parameter space: a 95 gev spin-0 resonance in the (b-l)ssm (2024), arXiv:2404.18653 [hep-ph].

[34] U. Ellwanger, C. Hugonie, S. F. King, and S. Moretti, NMSSM Explanation for Excesses in the Search for Neutralinos and Charginos and a 95 GeV Higgs Boson (2024), arXiv:2404.19338 [hep-ph].

[35] S. Yaser Ayazi, M. Hosseini, S. Paktinat Mehdiabadi, and R. Rouzbehi, Vector dark matter and LHC constraints, including a 95 GeV light Higgs boson, Phys. Rev. D **110**, 055004 (2024), arXiv:2405.01132 [hep-ph].

[36] A. Ahriche, 95 gev excess in the georgi-machacek model: Single or twin peak resonance, Physical Review D **110**, 10.1103/physrevd.110.035010 (2024).

[37] S. Bhattacharya, G. Coloretti, A. Crivellin, S.-E. Dahbi, Y. Fang, M. Kumar, and B. Mellado, Growing excesses of new scalars at the electroweak scale (2023), arXiv:2306.17209 [hep-ph].

[38] G. Aad *et al.* (ATLAS), Observation of a new particle in the search for the Standard Model Higgs boson with the ATLAS detector at the LHC, Phys. Lett. B **716**, 1 (2012), arXiv:1207.7214 [hep-ex].

[39] S. Chatrchyan *et al.* (CMS), Observation of a New Boson at a Mass of 125 GeV with the CMS Experiment at the LHC, Phys. Lett. B **716**, 30 (2012), arXiv:1207.7235 [hep-ex].

[40] J. F. Gunion, H. E. Haber, G. L. Kane, and S. Dawson, Errata for the Higgs hunter's guide (1992), arXiv:hep-ph/9302272.

[41] G. C. Branco, P. M. Ferreira, L. Lavoura, M. N. Rebelo, M. Sher, and J. P. Silva, Theory and phenomenology of two-Higgs-doublet models, Phys. Rept. **516**, 1 (2012), arXiv:1106.0034 [hep-ph].

[42] R. Benbrik, M. Boukidi, S. Moretti, and S. Semlali, Explaining the 96 GeV Di-photon anomaly in a generic 2HDM Type-III, Phys. Lett. B **832**, 137245 (2022), arXiv:2204.07470 [hep-ph].

[43] R. Benbrik, M. Boukidi, S. Moretti, and S. Semlali, Probing a 96 GeV Higgs Boson in the Di-Photon Channel at the LHC, PoS **ICHEP2022**, 547 (2022), arXiv:2211.11140 [hep-ph].

[44] A. Belyaev, R. Benbrik, M. Boukidi, M. Chakraborti, S. Moretti, and S. Semlali, Explanation of the Hints for a 95 GeV Higgs Boson within a 2-Higgs Doublet Model (2023), arXiv:2306.09029 [hep-ph].

[45] R. Benbrik, M. Boukidi, and S. Moretti, Superposition of CP-Even and CP-Odd Higgs Resonances: Explaining the 95 GeV Excesses within a Two-Higgs Doublet Model (2024), arXiv:2405.02899 [hep-ph].

[46] G. Branco, P. Ferreira, L. Lavoura, M. Rebelo, M. Sher, and J. P. Silva, Theory and phenomenology of two-higgs-doublet models, Physics Reports **516**, 1–102 (2012).

[47] B. Coleppa, F. Kling, and S. Su, Constraining type ii 2hdm in light of lhc higgs searches, Journal of High Energy Physics **2014**, 10.1007/jhep01(2014)161 (2014).

[48] I. F. Ginzburg and I. P. Ivanov, Tree-level unitarity constraints in the most general two higgs doublet model, Physical Review D **72**, 10.1103/physrevd.72.115010 (2005).

[49] G. Bhattacharyya and D. Das, Scalar sector of two-Higgs-doublet models: A minireview, Pramana **87**, 40 (2016), arXiv:1507.06424 [hep-ph].

[50] W. Porod, Spheno, a program for calculating supersymmetric spectra, susy particle decays and susy particle production at e+e− colliders, Computer Physics Communications **153**, 275–315 (2003).

[51] F. Staub, Exploring new models in all detail with `SARAH`, Advances in High Energy Physics **2015**, 1–126 (2015).

[52] J. Haller, A. Hoecker, R. Kogler, K. Mönig, T. Peiffer, and J. Stelzer, Update of the global electroweak fit and constraints on two-higgs-doublet models, The European Physical Journal C **78**, 10.1140/epjc/s10052-018-6131-3 (2018).

[53] P. Bechtle, D. Dercks, S. Heinemeyer, T. Klingl, T. Stefaniak, G. Weiglein, and J. Wittbrodt, Higgsbounds-5: testing higgs sectors in the lhc 13 tev era, The European Physical Journal C **80**, 10.1140/epjc/s10052-020-08557-9 (2020).

[54] H. Bahl, T. Biekötter, S. Heinemeyer, C. Li, S. Paasch, G. Weiglein, and J. Wittbrodt, Higgstools: Bsm scalar phenomenology with new versions of higgsbounds and higgssignals, Computer Physics Communications **291**, 108803 (2023).

[55] A. Tumasyan *et al.* (CMS), Search for a scalar or pseudoscalar dilepton resonance produced in association with a massive vector boson or top quark-antiquark pair in multilepton events at s=13 TeV, Phys. Rev. D **110**, 012013 (2024), arXiv:2402.11098 [hep-ex].

[56] P. Bechtle, S. Heinemeyer, T. Klingl, T. Stefaniak, G. Weiglein, and J. Wittbrodt, Higgssignals-2: probing new physics with precision higgs measurements in the lhc 13 tev era, The European Physical Journal C **81**, 10.1140/epjc/s10052-021-08942-y (2021).

[57] F. M. Borzumati and C. Greub, Two higgs doublet model predictions for $b \to x_s\gamma$ in nlo qcd, Physical Review D **58**, 10.1103/physrevd.58.074004 (1998).

[58] R. L. Workman and Others (Particle Data Group), Review of Particle Physics, PTEP **2022**, 083C01 (2022).

[59] W. Porod, F. Staub, and A. Vicente, A flavor kit for bsm models, The European Physical Journal C **74**, 10.1140/epjc/s10052-014-2992-2 (2014).

[60] CMS Collaboration, *Search for a standard model-like Higgs boson in the mass range between 70 and 110* GeV *in the diphoton final state in proton-proton collisions at* $\sqrt{s} = 13$ TeV, Tech. Rep. (CERN, Geneva, 2023).

[61] ATLAS Collaboration, *Search for diphoton resonances in the 66 to 110 GeV mass range using 140* fb^{-1} *of 13 TeV pp collisions collected with the ATLAS detector*, Tech. Rep. (CERN, Geneva, 2023) all figures including auxiliary figures are available at https://atlas.web.cern.ch/Atlas/GROUPS/PHYSICS/CONFNOTES/ATLAS-CONF-2023-035.

[62] A. Tumasyan *et al.* (CMS), Searches for additional Higgs bosons and for vector leptoquarks in $\tau\tau$ final states in proton-proton collisions at $\sqrt{s} = 13$ TeV, JHEP **07**, 073, arXiv:2208.02717 [hep-ex].

[63] J. Cao, X. Guo, Y. He, P. Wu, and Y. Zhang, Diphoton signal of the light higgs boson in natural nmssm, Physical Review D **95**, 10.1103/physrevd.95.116001 (2017).

[64] T. Biekötter, S. Heinemeyer, and G. Weiglein, 95.4 gev diphoton excess at atlas and cms, Phys. Rev. D **109**, 035005 (2024).

[65] T. Biekötter, S. Heinemeyer, and G. Weiglein, The cms di-photon excess at 95 gev in view of the lhc run 2 results, Physics Letters B **846**, 138217 (2023).

[66] ATLAS Collaboration (ATLAS), Combined measurements of Higgs boson production and decay using up to 139 fb^{-1} of proton-proton collision data at $\sqrt{s} = 13$ TeV collected with the ATLAS experiment (2021).

[67] A. Arhrib, R. Benbrik, and S. Moretti, Bosonic Decays of Charged Higgs Bosons in a 2HDM Type-I, Eur. Phys. J. C **77**, 621 (2017), arXiv:1607.02402 [hep-ph].

[68] A. Arhrib, R. Benbrik, R. Enberg, W. Klemm, S. Moretti, and S. Munir, Identifying a light charged Higgs boson at the LHC Run II, Phys. Lett. B **774**, 591 (2017), arXiv:1706.01964 [hep-ph].

[69] A. Arhrib, R. Benbrik, S. Moretti, A. Rouchad, Q.-S. Yan, and X. Zhang, Multi-photon production in the Type-I 2HDM, JHEP **07**, 007, arXiv:1712.05332 [hep-ph].

[70] A. Arhrib, R. Benbrik, H. Harouiz, S. Moretti, Y. Wang, and Q.-S. Yan, Implications of a light charged Higgs boson at the LHC run III in the 2HDM, Phys. Rev. D **102**, 115040 (2020), arXiv:2003.11108 [hep-ph].

[71] A. Arhrib, R. Benbrik, M. Krab, B. Manaut, S. Moretti, Y. Wang, and Q.-S. Yan, New discovery modes for a light charged Higgs boson at the LHC, JHEP **10**, 073, arXiv:2106.13656 [hep-ph].

[72] Y. Wang, A. Arhrib, R. Benbrik, M. Krab, B. Manaut, S. Moretti, and Q.-S. Yan, Analysis of $W^{\pm} + 4\gamma$ in the 2HDM Type-I at the LHC, JHEP **12**, 021, arXiv:2107.01451 [hep-ph].

[73] A. Arhrib, R. Benbrik, M. Krab, B. Manaut, S. Moretti, Y. Wang, and Q.-S. Yan, New Light $H^{\pm}$ Discovery Channels at the LHC, Symmetry **13**, 2319 (2021), arXiv:2110.04823 [hep-ph].

[74] Z. Li, A. Arhrib, R. Benbrik, M. Krab, B. Manaut, S. Moretti, Y. Wang, and Q. S. Yan, Discovering a light charged Higgs boson via $W^{\pm *} + 4b$ final states at the LHC (2023), arXiv:2305.05788 [hep-ph].